ICAS-84-2.8.2 GROUND EFFECT ON SLENDER WINGS AT MODERATE AND HIGH ANGLES OF ATTACK

J. Er-El* and D. Weihs**
Department of Aeronautical Engineering
Technion - Israel Institute of Technology
Haifa 32000, Israel

Abstract

The effect of ground proximity on a 60° delta wing at angles of attack of 10° to 31°, is studied by means of surface pressure measurements and oil flow visualization tests. Results show that ground effect increases the magnitude of the low pressure regions on the upper surface of the wing, induced by the leading edge vortices. The increase diminishes at high incidence where the effect of vortex breakdown is dominant. On the lower surface, ground effect increases the pressure. This increase becomes larger as the angle of attack increases. The overall result of ground effect is an increase in the normal force.

Nomenclature

c	-	Wing root chord
C_{NOR}	-	Normal force coefficient
$C_{nor}(\bar{x})$	-	Local normal force coefficient
C_p	-	Pressure coefficient $[(p-p_\infty)/q]$
h	-	Height of the wing trailing edge from the ground
h	-	Proximity ratio, (height h divided by trailing edge semi-span)
p	-	Pressure
q	-	Dynamic pressure
$s(\bar{x})$	-	Wing local semi-span
$\bar{x}$	-	Nondimensional chordwise coordinate $(\bar{x} = x/c)$
$\bar{y}$	-	Nondimensional local spanwise coordinate $[\bar{y} = y/s(\bar{x})]$
α	-	Angle of attack

Subscripts

∞	-	free stream
u	-	at the upper surface
l	-	at the lower surface

*Lecturer
**Professor

Introduction

Many modern high performance airplanes have slender wings. These make use of nonlinear lift effects, at moderate and high angles of incidence, to counter their low lift slope. One of the most critical phases of flight is take-off, where weight is largest and speeds are low. Thus high angles of attack are required in close proximity to the ground. It is therefore important to know the effects of ground proximity on the aerodynamics of the wing and the mechanisms by which they are produced. These effects are studied in this work on the basis of static pressure measurements on the wing surfaces.

The changes in the aerodynamic characteristics of wings as they approach the ground have been extensively studied. Most of these investigations dealt with high aspect-ratio planforms or two dimensional profiles where this effect was found to be significant[1,2]. Slender and delta wings have also been studied both experimentally and numerically. Force and moment measurements have been carried out on delta wings with various sweep angles by John[3], Kirkpatrick[4] and Kjelgaard and Paulsen[5]. The ground in these experiments was simulated by a stationary plate inserted in the wind-tunnel. All these studies dealt with forces only, and no pressure distribution measurements for slender wings were found in the literature. Numerical studies of ground effect on delta wings have been carried out by Fox[6], using a vortex lattice method, and by Hummel[7], using the lifting line and lifting surface theories. The ground in these calculations was represented by reflecting the image of the wing in the ground plane.

Previously existing numerical models and the overall force measurements do not deal with the angle of attack range where the effect of the leading edge vortices is significant. These vortices emanate from the wing apex and induce low pressure on the wing suction side[8,9,10], thus contributing to the lift. This contribution, which increases with angle of attack, is disrupted when the leading edge vortices undergo vortex breakdown. The conditions for its occurrence depend on the leading edge sweep angle, in addition to the angle of attack[11]. The structural change due to vortex breakdown inhibits the development of the suction peaks on the upper surface and consequently reduces the contribution of the leading edge vortices to the lift. The effects of ground proximity in these cases are also expected to be influenced by the leading edge vortices. These influences should be manifested in the pressure distributions on the wing surfaces and should give an indication on the aerodynamic mechanisms which produce the ground effect.

The purpose of the present study is to investigate the effects of ground proximity on

delta wings at moderate and high angles of attack on the basis of surface pressure distributions, supplemented by oil-flow visualization tests.

Experimental Setup and Procedure

The experiments reported in this study were carried out in the subsonic wind tunnel of the Aeronautical Research Center at the Technion. The experimental setup consists of the slender wing model, the pressure reading system and the ground simulation board. The experiments consisted of detailed surface pressure measurements and oil-flow visualization tests.

The wing used in this study is a sharp-edged delta wing of 60° sweep angle, root chord length of 24.6 cm and uniform thickness of 4.6 mm (Fig. 1). The wing has two flat surfaces and a symmetrical wedge-shaped (apex angle of 30°) leading edge and trailing edge. Pressure tubes, of 0.6 mm inside diameter, are embedded in the wing and 130 ports for static pressure measurements are drilled on the upper surface. These holes are located at the junctions of 10 rays radiating from the apex and 14 spanwise rows (Fig. 2). Each row contains 10 holes, except for the three rows closest to the apex where restricted space necessitated the presence of less holes per row. Consequently, the first row contains 6 holes and the second and third rows contain 7 holes each.

The distribution of pressure holes was designed for high spatial resolution for the given number of ports. Consequently, flow symmetry was used to concentrate the holes on one side of the upper surface (the starboard side). In addition, the spanwise spacings, with respect to the local span, are smaller in the area below the leading edge vortex trajectories on the wing, where large spanwise pressure gradients were expected.

The pressure measurement system is based on three 48 ports scanivalve SGM modules, each connected to a Statham pressure transducer type 6 or 96. A schematic diagram of the system is given in Fig. 3. The surface pressure readings along with the readings of a calibrated pressure and the free-stream kinematic pressure are processed by computer.

The ground was simulated by a flat board 1.25 cm thick and 150 cm long with a sharp leading edge, spanning the width of the wind tunnel (100 cm) parallel to the wind tunnel floor. The experiments were carried out with the wing trailing edge placed about four chords (100 cm) downstream from the leading edge of the board. An overall view of the system with the ground board is given in Fig. 4.

In oil-flow visualization tests which were made on the ground plate the flow near the ground appears uniform, laminar and with no indications of boundary layer separation.

The displacement thickness of the ground plane boundary layer in the pressure measurement experiments is approximately 0.09 cm at a distance of 100 cm downstream from the leading edge of the board (and below the trailing edge of the wing). ($Re \cong 1.6 \cdot 10^6$, based on the free-stream velocity of 30 m/sec). The displacement thickness introduces a small reduction in the ground height. This reduction is negligible compared to the minimum value of h=5 cm which was used in the experiments.

In a typical experiment the wing was set at a prescribed angle of attack, and pressure measurements on the upper surface were performed for a series of ground heights. The wing was then turned over so that the pressure measurement surface became the lower surface, and data were taken for the same series of heights. This procedure was repeated for a series of angles of attack to obtain the full data set. The average error in the pressure reading was estimated from a repeated test. The average difference between the readings of the original and repeated tests is 0.005 C_p and the standard deviation is 0.025 C_p.

The pressure values were used to compute the pressure coefficients at the measurement points on the upper and lower surfaces. The spanwise profiles of the pressure coefficients were numerically integrated using the Romberg integration scheme to produce the chordwise normal force loading

$$C_{nor}(\bar{x}) = \frac{1}{s(1)} \int_0^{S(\bar{x})} [C_{p,l} - C_{p,u}] dy \qquad (1)$$

and the normal force coefficient was obtained by a numerical integration of $C_{nor}(\bar{x})$

$$C_{NOR} = \int_0^1 C_{nor}(\bar{x}) d(\bar{x}) \qquad (2)$$

The flow near the ground surface and the wing surfaces was studied by means of oil-flow patterns. The surfaces were painted by a mixture of one volumetric unit of fluorocentric powder and 3 volumetric units of petroleum and was exposed to the flow for about 2 minutes until the pattern dried out.

Results and Discussion

Surface pressures

The surface pressure measurements reported here were conducted at angles of attack of α = 10°, 15°, 17.5°, 21°, 25° and 31° and a range of ground proximity ratios of $\bar{h}$ = 0.365, 0.730, 1.095, 1.460, 1.825 and 2.336, (h = 5 to 32 cm).

Figures 5 to 8 feature the spanwise distributions of the pressure coefficients on the upper and lower surfaces of the wing for the two extreme proximity ratios $\bar{h}$ = 0.365 and 2.336 and at the angles of attack of α = 10°, 15°, 25° and 31°. The proximity ratios were selected to represent the case of pronounced ground effect ($\bar{h}$ = 0.365) and the case closest to that of free flight ($\bar{h}$ = 2.336). The angles highlight the various regimes in the range of incidences studied here.

i) At $\alpha = 10^\circ$ (Fig. 5) nonlinear lift is not fully developed, and there are no signs of vortex breakdown.

ii) At $\alpha = 17.5^\circ$ (Fig. 6) vortex breakdown appears at the trailing edge area.

iii) At $\alpha = 25^\circ$ (Fig. 7) vortex breakdown has affected the rear half of the leading edge vortices on the planform.

iv) At $\alpha = 31^\circ$ (Fig. 8) the leading edge vortices are completely in the post-breakdown configuration.

The spanwise pressure distributions are shown for 3 representative chordwise stations at approximately 40%, 70% and 90% chord of the root chord length (rows 4, 9 and 13 in Fig. 2).

Figures 5-8 serve as a general framework for the analysis of the pressure data. These and similar measurements at other angles and proximity ratios will now be used to first describe the pressure field on the planform, and then to highlight effects of ground proximity. Upper and lower surface measurements are discussed separately to enable pinpointing specific effects.

Pressure distributions on the suction side

The pressure distributions obtained on the suction side (the upper surface) for $\bar{h} = 2.336$ are reminiscent of those found in previous studies of delta and other slender planforms in unbounded flow[8,9,10]. The pressure coefficients $C_{p,u}$, are negative, and are dominated by the contribution of the leading edge vortices (the large negative peaks in Figs. 5-8). This effect is largest near the apex and decreases in the downstream direction. Comparison of the spanwise $C_{p,u}$ profiles for the same rows in Figs. 5 through 8 shows that the magnitude of the suction peaks increases with angle of attack.

The effect of ground proximity on the suction side is manifested in the increased absolute values of $C_{p,u}$ (Figs. 5-8). This increase, which is largest in the regions of maximum suction, can be explained on the basis of a classical ground effect model. This model considers the effect of ground proximity as the interaction of a wing captive vortex and its image in the ground. This is generalized here to describe the interaction of the leading edge vortices and their images, as shown schematically in Fig. 9. This interaction can be best shown by considering the effect of the pair of the image vortices on one of the leading edge vortices - the right one, for example. The image vortex underneath it tends to displace it outwards whereas the left image vortex induces an upwards and inwards displacement. The distance between the real vortex and the left image vortex is larger than the distance between the real one and the right image vortex. Consequently, the displacement due to the left image vortex is smaller than the displacement due to the right image vortex. The resultant effect of the image vortices on the real ones is an outboard and upward displacement. The upward component of the displacement is accompanied by an increase in their circulation. This increase is necessary in order to maintain their equilibrium in their new positions as predicted by analytical models of the flow over delta wings[12]. The increased circulation results in an increase in the suction generated by the leading edge vortices which appears as an increase in the absoute values of C_p on the upper surface, underneath the leading edge vortices (Figs. 5-8). The increased suction due to ground effects is unique to slender wings where the leading edge vortices are located over the wing surface and affect the flow directly. In two-dimensional or high aspect ratio wings, for example, the suction is reduced due to ground effect[2]. This reinforces the model which associates the increased suction due to ground effect in delta wings with the interaction of the leading edge vortices and their image.

A quantitative account of the increased suction due to ground effect appears in Fig. 10 where the values of $C_{p,u}$ along the rays nearest to the suction peaks are plotted for $\alpha = 10^\circ$, 17.5° and 25°. In general, the absolute values of $C_{p,u}$ decrease in the downstream direction from their largest values near the apex towards zero at the trailing edge. The dip observed in the $C_{p,u}$ curves near the apex at $\alpha = 10^\circ$ and 17.5° can be attributed to the local structure of the pressure field there, which is the result of the geometry of the leading edge and the relative position of the pressure peak to the nearest pressure hole. This dip disappears at higher angles of attack when this relative position changes due to the displacement of the leading edge vortices.

Figure 10 also shows that the increase due to ground effect appears as an almost constant addition to $C_{p,u}$ along the rays, except near the apex. The pressure gradients there are very steep and a slight change in the relative position of the leading edge vortex to the nearest pressure hole on the ray may result in large changes in the pressure readings. For $\bar{x} > 0.4$, the increase is larger at $\alpha = 17.5^\circ$ than at the other angles of attack shown in Fig. 10. This can be attributed to the fact that at the higher angle (25°) the leading edge vortices are strongly affected by vortex breakdown and therefore the effect of ground proximity on the interaction of the real and image vortices is weaker than at $\alpha = 17.5^\circ$. At the lower angle (10°), the leading edge vortices are weaker than at $\alpha = 17.5^\circ$ and therefore the effect of the interaction mechanism must also be weaker.

The effect of ground proximity on the suction peaks is weakest at $\alpha = 31^\circ$ (Fig. 8) where the effect of vortex breakdown is largest.

The pressure side

The pressure side of the wing (the lower side) is characterized by positive pressure coefficients on most of the wing (Figs. 5-8). The magnitude of the pressure coefficients on this side are considerably smaller than those on the suction side in the angle of attack range considered in this study. Consequently, the contribution of this surface to the lift is also smaller than the contribution of the upper surface.

The spanwise profiles of the pressure coefficients on the pressure side, which faces the free stream flow, are more uniform than those on the suction side, which is strongly affected by the leading edge vortices. A quantitative measure of the pressure coefficients on the lower surface and the effect of ground proximity on them appears in the curves of $C_{p,l}$ along ray No. 1 ($\bar{y} = 0.2$) for $\alpha = 10.^\circ$, 17.5° and $25.^\circ$ (Fig. 11). The values of $C_{p,l}$ are largest near the apex, due to the slowdown of the flow in this region, and decrease in the downstream direction, as the flow accelerates, to negative values near the trailing edge. Figure 11 also shows that the values of $C_{p,l}$ increase as the angle of attack increases. The addition to $C_{p,l}$ is largest near the apex and decreases in the downstream direction.

Introduction of the ground plane increases the values of $C_{p,l}$ (Fig. 11). This is probably a consequence of the reduction in the mass flow between the wing and the ground as the wing approaches the ground. This pressure increase appears as an almost constant addition to the values obtained in ground-free tests at the same angle of attack. The addition due to ground affect increases with angle of attack; for example: as the angle of attack increases from 10° to 25° the addition increases by a factor of 1.5 to 2. The increase in $C_{p,l}$, due to the same increase in angle of attack, is approximately by a factor of 4.

An additional phenomenon which is observed in the spanwise pressure distributions on the pressure side (Fig. 5 through 8) is the dip in the spanwise profiles near the trailing edge, which is represented in these figures by row No. 13 (see Fig. 2). The minimum values of $C_{p,l}$ in the dips are located below the suction peaks and the leading edge vortices. This dip also appears, in a weak form, in the ground-free tests and becomes more pronounced as the wing approaches the ground.

This phenomenom is probably associated with the effect of the leading edge vortices, in the ground-free cases, in addition to the effect of their image in the ground, when ground proximity affects the wing. apparently, the suction induced by the leading edge vortices on the suction side, "leaks" into the trailing edge region on the pressure side. When ground effect exists, the image vortices induce additional suction in this region, in a manner similar to the effect of the leading edge vortices on the suction side.

The normal force

As shown in the preceding sections, ground effect increases the suction on the suction-side and the pressure on the pressure-side. The combined effect of ground proximity is thus to increase the pressure difference between both sides of the wing, the wing loading and the normal force acting on it.

Figure 12 features this effect on the chordwise loading, $C_{nor}(\bar{x})$ for $\alpha = 10^\circ$, 17.5° and 25°. The $C_{nor}(\bar{x})$ profiles tend to zero at the apex and the trailing edge and attain a maximum at the planform center for ($\bar{x} \cong 0.7$). The tendency to zero as $\bar{x} \to 0$ is the result of the decrease in the wing span to zero. The tendency to zero at $\bar{x} \to 1$ is the result of the need to satisfy the Kutta condition at the trailing edge. Consequently, the main contribution to the normal force comes from the central portion of wing. Ground effect increases the wing loading; this increase tends to zero in the same manner as $C_{nor}(\bar{x})$ curves does.

The normal force coefficients, C_{NOR}, is obtained by a chordwise integration of $C_{nor}(x)$ (Eq. (2)). Figure 13 features the variations of the normal force with ground proximity, by comparison to C_{nor} in free flow for $\alpha = 10.^\circ$, 17.5° and 25°. Evidently, as the wing approaches the ground, the effect of ground proximity increases. The effect is noticeable for $\bar{h} < 1$.

Figure 14 features the variations of the normalized C_{NOR} with angle of incidence for $\bar{h} = 0.365$. The maximum normalized extra C_{NOR}, approximately 13.4%, is obtained at $\alpha \cong 14^\circ$. At this angle, breakdown of the leading edge vortices appears at the trailing edge of a 60° delta wing[11], and the relative contribution of the leading edge vortices is largest in this angle; i.e. vortex breakdown tends to reduce the ground effect, again showing that the major influence of the ground is on the leading edge vortices. In comparison, the normalized extra C_{nor} obtained from the empirical correlation proposed by Kuchemann[13], at low angles of attack, is 16.2%.

Figure 15 features the normal force coefficients curves as a function of angle of attack for $\bar{h} = 0.365$ and 2.336. The C_{NOR} curve obtained by Earnshaw and Lawford[14] for a 60° sweep angle delta wing in free stream is included, for comparison. The results of Ref. 14 are in good agreement with the present results for $\bar{h} = 2.336$.

Oil flow visualization

The oil flow pattern on the ground plate provides an indication of the effect of the wing on the flow near the ground. Figures 16 and 17 feature the oil flow patterns obtained for $\alpha = 17.5^\circ$ and proximity ratios of 0.365 and 2.336, respectively. At the smallest proximity ratio (Fig. 16), the flow near the ground diverges to counter the downstream reduction in the cross-sectional area available for the flow between the wing and the ground. Downstream of the trailing-edge, the flow near the ground is affected by the induced velocities of the leading edge vortices. The upstream influence of the wing extends approximately half a chord from the apex.

The effects of the wing on the ground are weaker as $\bar{h}$ increases and at $\bar{h} = 2.336$ the streamlines parallel (Fig. 17).

Concluding Remarks

The normal force on slender wings increases as the wing approaches the ground. This increase is the result of higher pressures on the lower surface, due to the reduced mass flow between the wing and the ground, and of lower pressures on the upper surface, due to the augmenting effect

of the ground on the leading edge vortices. Thus, a larger pressure difference between the wing surfaces, and consequently a larger normal force, is obtained.

Vortex breakdown reduces the relative contribution of the upper surface to ground effect and a maximum normalized increase of 13.4% is obtained at $\alpha \cong 14^{\circ}$. This value is typical of take-off and landing angles of slender wing aircrafts. These angles, however are dictated by ground clearance constraints, rather than by aircraft aerodyanmics.

Acknowledgement

The authors would like to acknowledge Mr. S. Kusinski's assistance in this study. This research was partially supported by the Technion V.P.R. Fund - L. Rogov Aeronautical Research Fund.

References

1. Tomika, S., Hasimoto, Z. and Urano, K.: "The Forces Acting on an Airfoil of Approximate Joukowski Type in a Stream Bounded by a Plane Wall". Quart. J. Mech. Appl. Math., Vol. 4, 1951, pp. 289-307.

2. Bagley, J.A.: "The Pressure Distribution on Two Dimensional Wings Near the Ground". ARC R and M No. 3238, 1961.

3. John, H.: "Systematische Sechskomponenten-Windkanalmessungen an Schiebenden Flugeln in Bodennahe. Teil III: Deltaflugel". Berichte des Inst. fur Flugtechnik der TH Darmstadt, 1965.

4. Kirkpatrick, D.L.I.: "Experimental Investigation of the Ground Effect on the Subsonic Longitudinal Characteristics of a Delta Wing of Aspect Ratio 1.616". RAE-TR 66179, 1966.

5. Kjelgaard, S.O., and Paulsen, J.W.: "Effect of Sweep and Aspect Ratio on Longitudinal Aerodynamics of a Spanloader Wing In and Out of Ground Effect". NASA TM-80199, 1981.

6. Fox, C.H.: "Prediction of Lift and Drag for Slender Sharp Edged Delta Wings in Ground Proximity". NASA TN D-4891, January 1969.

7. Hummel, D.: "Nichtlineare Tragflugeltheorie in Bodennahe. Z.F.W. Vol. 21, 1973, pp. 425-442.

8. Kirkpatric, D.L.I.: "Analysis of Static Pressure Distribution on a Delta Wing in Subsonic Flow". RAE TR-68217, 1968.

9. Hummel, D.: "On the Vortex Formation over a Slender Wing at Large Angles of Incidence". AGARD CP-247, Paper No. 15, 1979.

10. Chevemukin, G.A., Tuneva, E.A. and Piokin, E.J.: "Flow Past Small Aspect-Ratio Delta Wing with Vortex Breakdown". Aviatsionnia Technika, Vol. 21, No. 4, 1978, pp. 162-167.

11. Wentz, W.H. and Kohleman, D.L.: "Wing Tunnel Investigations of Vortex Breakdown on Slender Sharp-Edged Wings", Rep. FRL 69-013, Univ. of Kansas Center for Research, Lawrence, Kansas, 1966.

12. Smith, J.H.B.: "Improved Calculations of Leading-Edge Separation from Slender Delta Wings", RAE TR-66070, 1966.

13. Kuchemann, D.: "The Aerodynamic Design of Aircraft", Pergamon Press, 1978.

14. Earnshaw, P.B. and Lawford, J.A.: "Low-Speed Wind-Tunnel Experiments on a Series of Sharp-Edged Delta Wings". ARC R and M No. 3424, 1966.

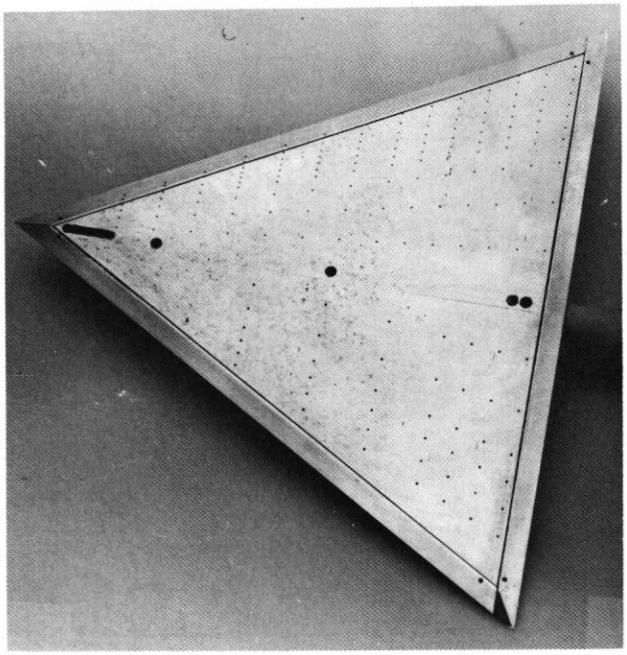

Fig. 1. The delta wing model.

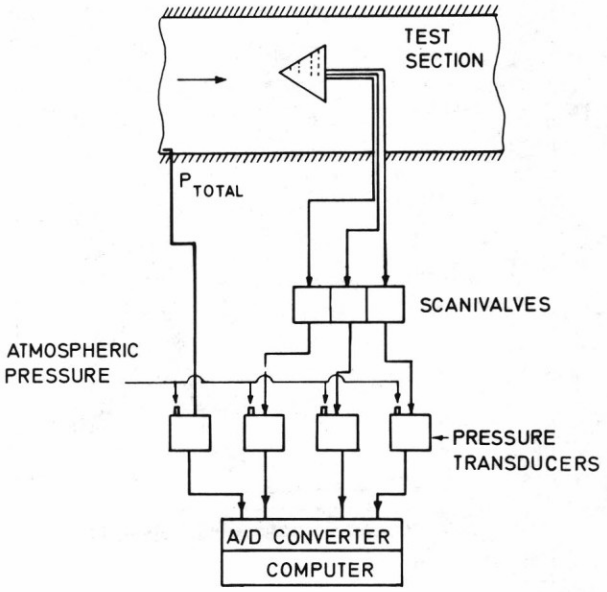

Fig. 3. Schematic diagram of the experimental setup.

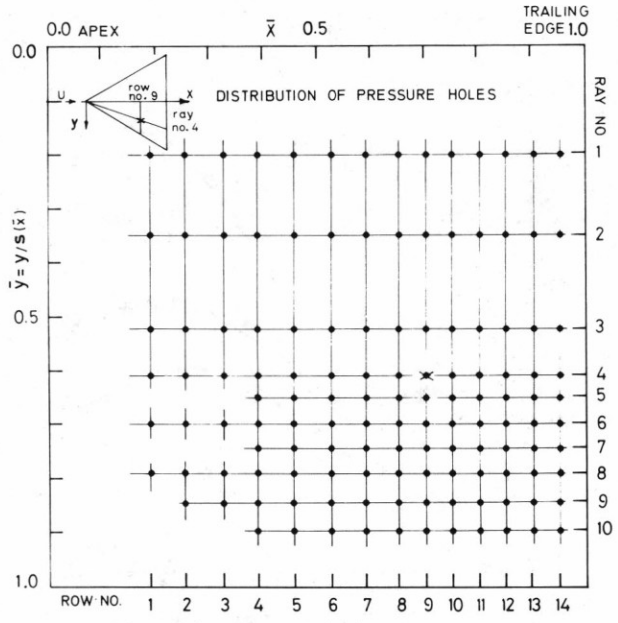

Fig. 2. Map of the pressure holes on the wing surface. The triangular wing planform is shown in a transformed rectangular plane. The pressure hole at the junction of ray No. 4 and row No. 9 is denoted by x in the map and the insert.

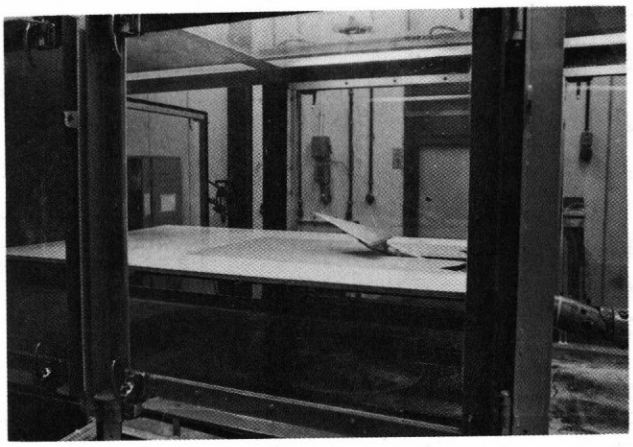

Fig. 4. An overall view of the wing model and the ground board in the wind-tunnel.

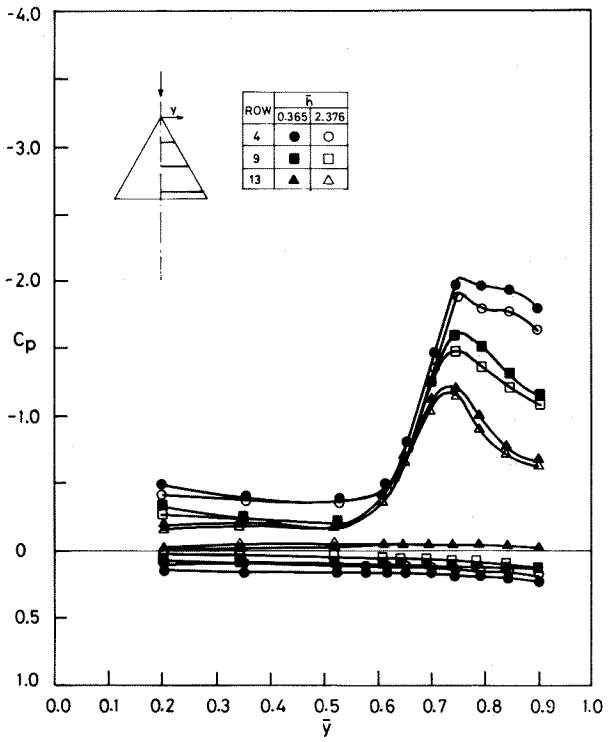

Fig. 5. Spanwise pressure distributions at $\alpha=10^{\circ}$.

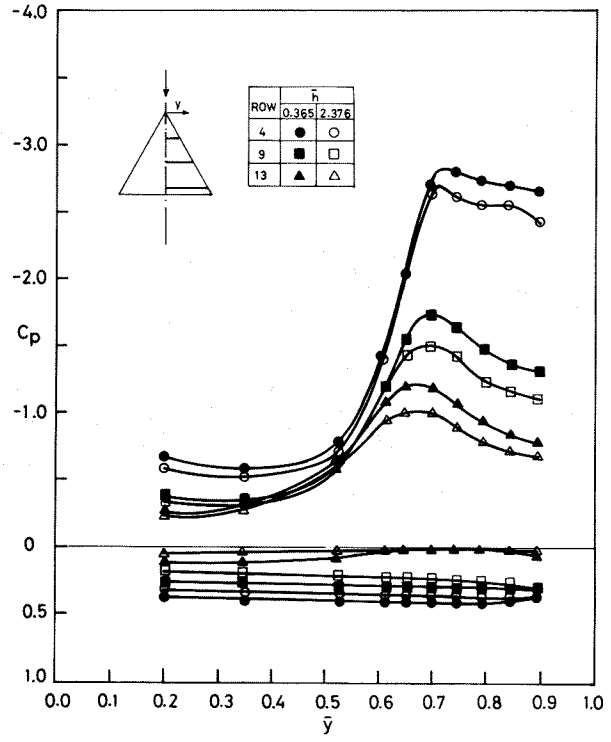

Fig. 6. Spanwise pressure distributions at $\alpha=17.5^{\circ}$.

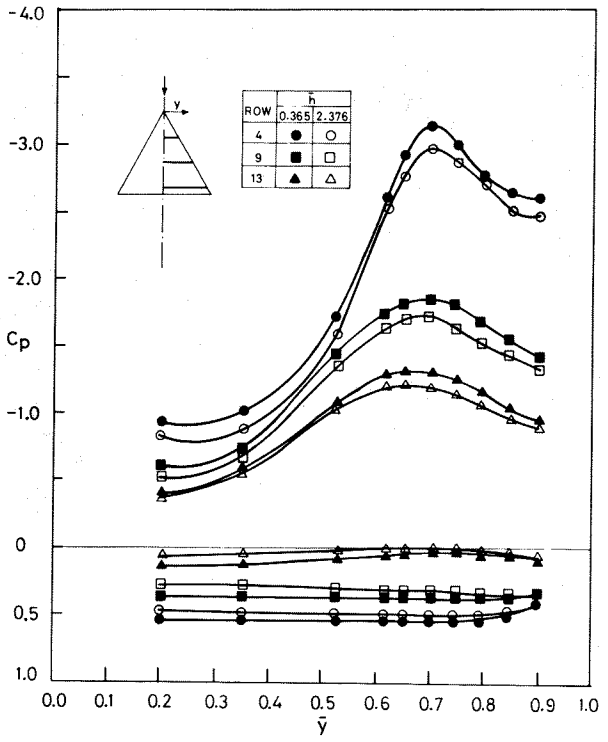

Fig. 7. Spanwise pressure distributions at $\alpha=25^{\circ}$.

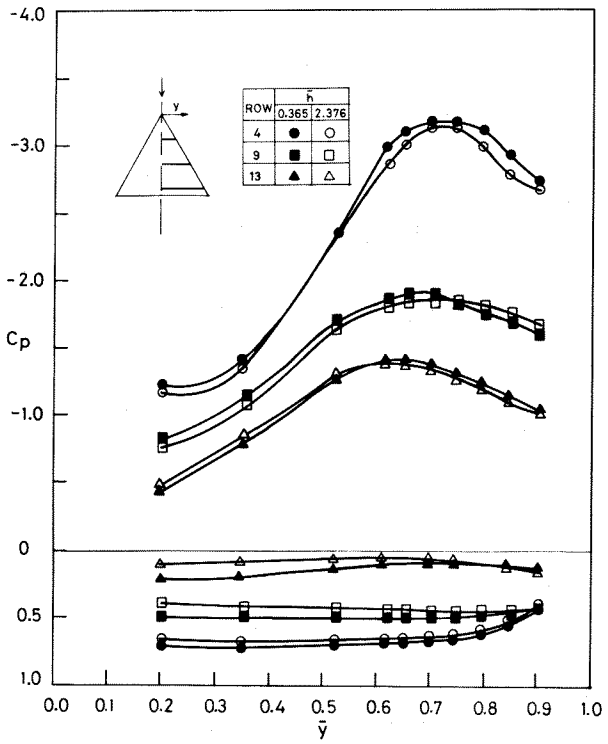

Fig. 8. Spanwise pressure distributions at $\alpha=31^{\circ}$.

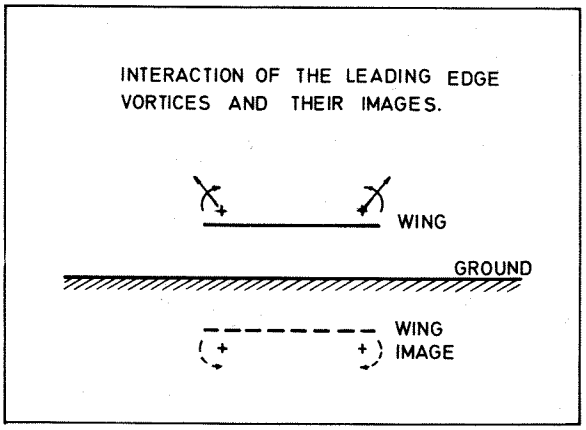

Fig. 9. Schematic rear view of the wing with its leading edge vortices and their image in the ground. The directions of the displacements of the real vortices due to the mutually induced velocities is denoted by the straight arrows.

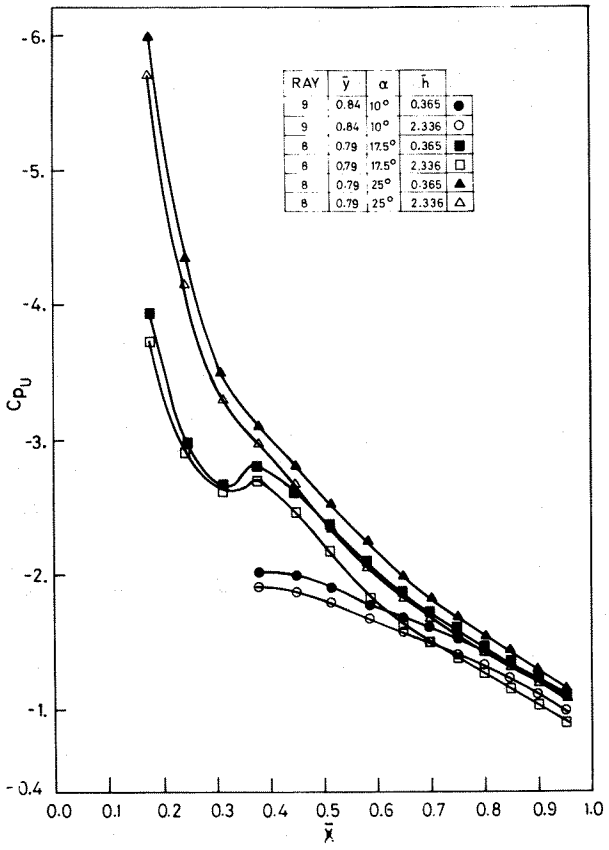

Fig. 10. The chordwise $C_{p,u}$ profiles along the rays near the suction peaks.

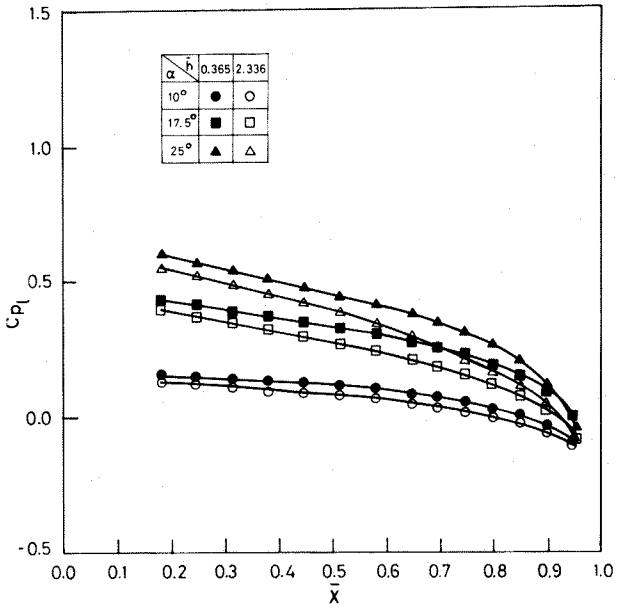

Fig. 11. The chordwise $C_{p,l}$ profiles along ray No. 1 ($\bar{y}\cong 0.2$).

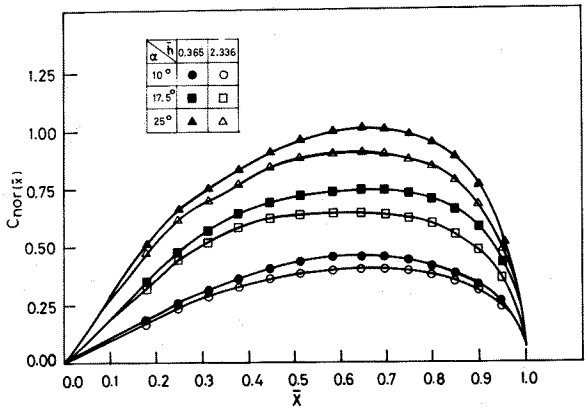

Fig. 12. The chordwise wing loading.

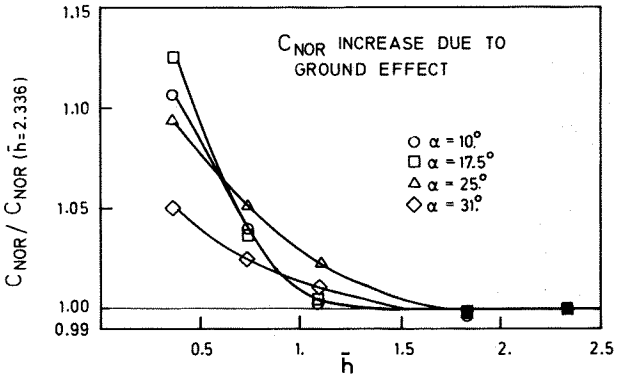

Fig. 13. Effect of ground proximity on the normalized C_{nor}.

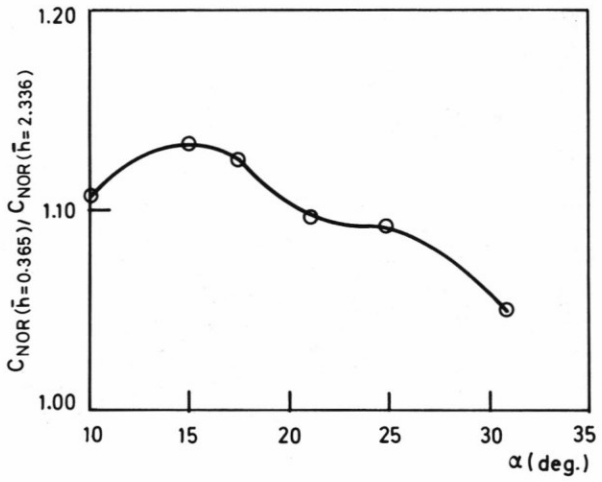

Fig. 14. Normalized C_{NOR} at $\bar{h}$ = 0.365 versus angle of attack.

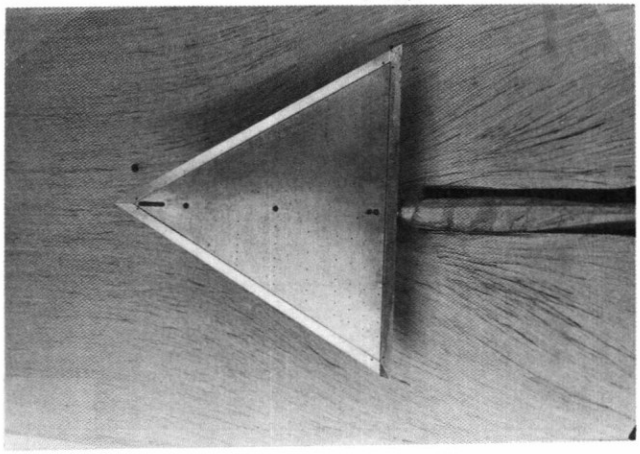

(a)

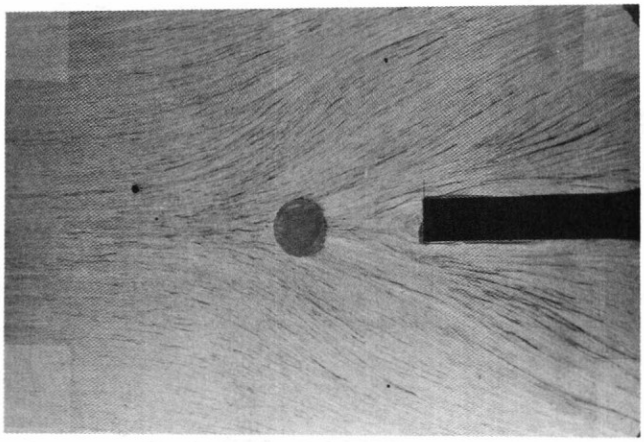

(b)

Fig. 16. Oil flow pattern on the ground plate, $\bar{h}$ = 0.365 and α = 17.5°.
(a) Before the wing has been removed.
(b) After the wing has been removed.

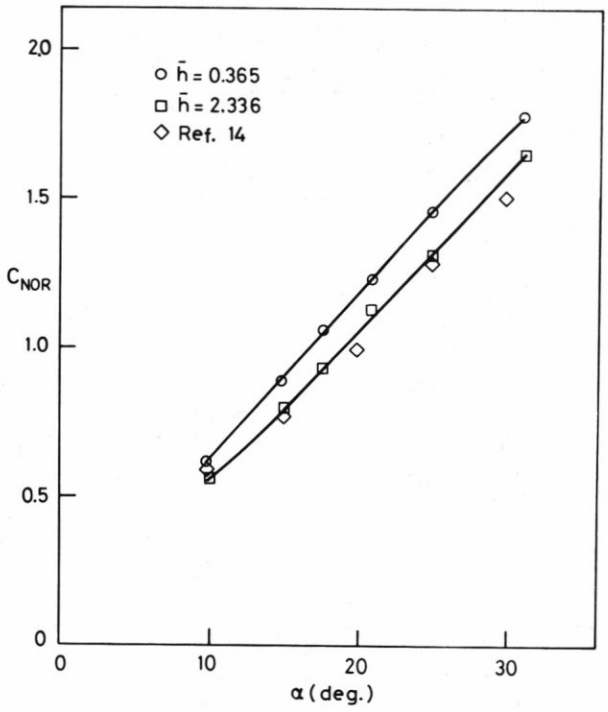

Fig. 15. Normal force coefficient versus angle of attack.

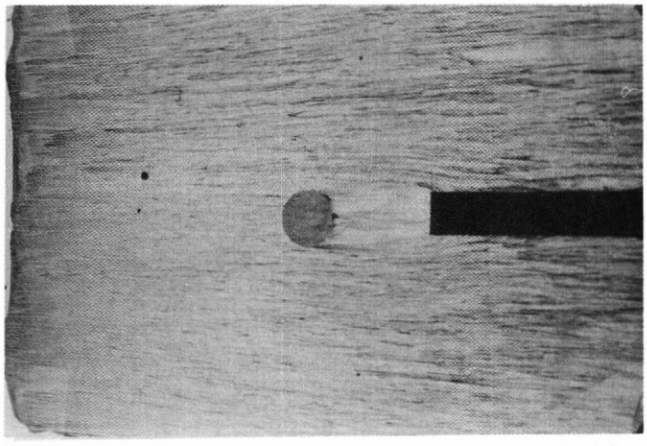

Fig. 17. Oil flow pattern on the ground plate, $\bar{h}$ = 2.336 and α = 17.5°. The wing has been removed.